IEEE Access
Multidisciplinary | Rapid Review | Open Access Journal

Received 9 March 2026, accepted 24 March 2026, date of publication 27 March 2026, date of current version 1 April 2026.

Digital Object Identifier 10.1109/ACCESS.2026.3678351

RESEARCH ARTICLE

Implementation and Evaluation of Hierarchical Beam Selection Algorithm for mmWave WPT Systems

JAE CHEOL PARK[1], JUNGICK MOON[1], AND JUNIL CHOI[2], (Senior Member, IEEE)
[1]Radio Environment & Monitoring Research Section, Electronics and Telecommunications Research Institute, Daejeon 34129, South Korea
[2]School of Electrical Engineering, Korea Advanced Institute of Science and Technology, Daejeon 34141, South Korea

Corresponding author: Junil Choi (junil@kaist.ac.kr)

This work was supported by the Institute of Information & Communications Technology Planning & Evaluation funded by Korean Government (MSIT) through the Development of Multi-Meter Level Radio Beam Wireless Charging Technology Based on Millimeter Waves under Grant RS-2024-00398981.

ABSTRACT In this paper, the millimeter wave (mmWave) wireless power transfer (WPT) system is considered where the wireless charging station (WCS) operates without prior knowledge of the wireless charging device (WCD)'s location. A hierarchical beam selection algorithm is proposed, which employs hierarchical beams with varying beamwidths to determine the optimal beam for the WCD while mitigating error propagation (EP) across levels. The proposed algorithm consists of the beam identification process and the verification process. In the beam identification process, the WCS identifies the beam that achieves the highest received signal strength indicator (RSSI). In the verification process, the WCS validates the selected beam using the verification beam set, which is constructed based on the beam with the second-highest RSSI. This process mitigates EP across hierarchical levels. The proposed algorithm is implemented on the commercial mmWave RF module, and its performance is evaluated through experiments in the indoor laboratory environment.

INDEX TERMS Hierarchical beam selection, millimeter waves (mmWave), wireless power transfer (WPT), verification process, experimental validation.

I. INTRODUCTION

Millimeter waves (mmWaves) are radio waves with frequencies ranging from 24 GHz to 300 GHz, and they are widely used in various applications such as wireless communications, radar systems, and wireless power transfer (WPT) systems [1], [2], [3], [4], [5]. In WPT systems, the wireless charging station (WCS) transmits radio frequency (RF) signals, and then the wireless charging device (WCD) harvests electrical energy from the received RF signals. To overcome the severe path loss of mmWave signals, the mmWave WPT systems utilize beamforming technologies that enable efficient power delivery over short ranges of 1 to 3 meters under line-of-sight (LoS) conditions [6], [7], [8].

Several studies have investigated beamforming techniques for mmWave WPT systems [9], [10], [11]. Unlike mmWave communication systems that can exploit rich channel state information, mmWave WPT systems typically rely on limited feedback information, such as the received signal strength indicator (RSSI) or harvested energy measurements. Specifically, when the location of the WCD is unknown at the WCS, accurately aligning a narrow beam between the WCS and the WCD requires high computational complexity. These characteristics pose unique challenges for beam selection in practical mmWave WPT systems and motivate the development of efficient beam selection algorithms tailored to RSSI-based and location-unaware scenarios.

To reduce the computational complexity of beam alignment, various beam selection approaches have been investigated, including hierarchical and learning-based methods [12], [13], [14], [15]. While these approaches can reduce beam search complexity compared to exhaustive search, conventional hierarchical methods may suffer from performance degradation due to error propagation (EP) across hierarchical

The associate editor coordinating the review of this manuscript and approving it for publication was Zaharias D. Zaharis.

TABLE 1. Comparison of beam selection methods for mmWave WPT systems.

Method	Strategy	Overhead	Robustness	Training	Complexity	EP Mitigation
Exhaustive Search	Full beam search	High	High	None	High	N/A
Conventional Hierarchical	Coarse-to-fine search	Low	Low	None	Low	No
Learning-based Methods	Data-driven prediction	Medium	Medium–High	Required	Medium–High	Implicit
Proposed Algorithm	Hierarchical search w/ verification	Medium–Low	Medium–High	None	Medium–Low	Yes

levels, whereas learning-based approaches often require prior data collection and model training, which can increase implementation complexity and limit adaptability in dynamic environments. These limitations motivate the need for a lightweight and training-free beam selection algorithm that is robust to practical uncertainties in mmWave WPT systems.

In this paper, the mmWave WPT system is considered, where the WCS operates without prior knowledge of the WCD's location. The WCD is assumed to be a low-power IoT sensor that operates intermittently and requires periodic wireless charging in the indoor environments such as smart buildings or factories [2], [17]. A hierarchical beam selection algorithm is proposed to maximize the harvested energy at the WCD under the predefined beam set constraint at the WCS. The major contributions of this paper are summarized as follows:

- A hierarchical beam selection algorithm is proposed that incorporates a verification process to mitigate EP across hierarchical levels in mmWave WPT systems, which, to the best of our knowledge, has not been explicitly addressed in conventional hierarchical beamforming methods [12], [13].
- The proposed algorithm is implemented on a commercial mmWave RF module and evaluate its performance in an indoor laboratory environment.
- It is experimentally demonstrated that the proposed algorithm identifies the same optimal beam as exhaustive search while requiring fewer beam allocations.
- It is shown that the proposed algorithm achieves higher RSSI values than conventional hierarchical beam selection algorithms.

The remainder of this paper is organized as follows. The related works are introduced in Section II. The system model is described in Section III. The proposed hierarchical beam selection algorithm is presented in Section IV. The implementation of the proposed algorithm on the commercial mmWave RF module is described in Section V. Experimental results are provided in Section VI. Finally, Section VII concludes the paper.

II. RELATED WORK

This section reviews related work on mmWave beamforming and beam selection techniques relevant to mmWave WPT systems.

A. BEAMFORMING

The random energy beamforming and several intelligent schemes that steer the beam to specific areas by considering receiver locations were proposed for mmWave wireless powered sensor networks, enabling efficient energy transfer in large-scale networks [9]. The directional WPT scheme using mmWave power beacons with beam training was proposed to improve power coverage and system performance in [10]. The dynamic multi-steerable energy beamforming scheme, which optimizes beam splitting and transmission resources, was proposed to maximize energy harvesting and energy efficiency for mmWave wireless-powered communication networks (WPCNs) in [11].

B. HIERARCHICAL BEAM SELECTION

The beamforming schemes with hierarchical search structure have been proposed to reduce computational complexity in [12], [13]. The hierarchical multi-resolution codebook design and adaptive beamforming sequence proposed in [12] jointly minimize training overhead and maximize the average data rate under time constraints, using a phase-shifted discrete Fourier transform (DFT) approach. In [13], the generalized hierarchical codebook design and dynamic beam training method were presented, which exclude estimated multipath components to improve success detection and reduce training overhead in mmWave massive MIMO systems However, the algorithms in previous studies did not consider the issue of EP across levels caused by the beam selection errors.

C. LEARNING-BASED BEAM SELECTION

The deep learning-based hierarchical beam alignment method was proposed to enhance beam alignment accuracy and reduce signaling overhead by employing learned probing codebooks for coarse-to-fine beam search [14]. The deep learning-based beam recommendation method was proposed to improve beam alignment accuracy and efficiency by leveraging an enhanced channel knowledge map (En-CKM) in mmWave environments [15]. The lightweight deep learning-based beam prediction method was proposed to enable real-time mmWave beam alignment by leveraging low-complexity neural networks and location-related side information, thereby reducing beam training overhead while maintaining prediction accuracy [16]. However, such approaches typically rely on prior data collection and model training, often assisted by auxiliary information. In contrast, a low-complexity hierarchical beam selection algorithm is proposed that mitigates EP without relying on learning.

D. COMPARISON WITH PROPOSED ALGORITHM

Table 1 summarizes the trade-offs among representative beam selection approaches for mmWave WPT systems. While

TABLE 2. List of main symbols.

Symbol	Description
L	Total levels of beams
$\mathbf{b}_{\mathrm{t}}$	Transmit beamformer
$\mathbf{c}_{\mathrm{r}}$	Receive combiner
η	Energy conversion efficiency
$N_{l,c}$	Number of candidate beams at level l
$N_{l,v}$	Number of verification beams at level l
$\mathbf{b}_{l,c}$	c-th candidate beam at level l
$\mathbf{b}_{l,v}$	v-th verification beam at level l
$\mathcal{C}_{l,i^*_{l+1}}$	Candidate beam set at level l
$\mathcal{V}_{l,i^\dagger_{l+1}}$	Verification beam set at level l

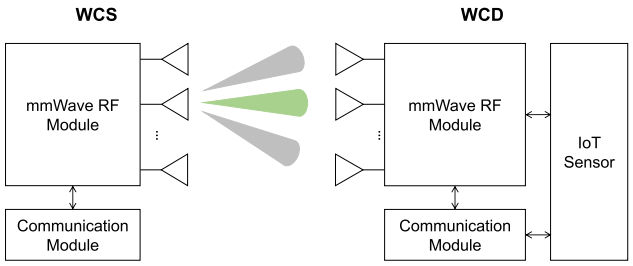

FIGURE 1. mmWave WPT systems.

exhaustive search offers high robustness at the cost of very high overhead and complexity, conventional hierarchical methods reduce overhead but suffer from low robustness due to EP. Learning-based approaches can improve robustness, but they typically introduce higher implementation complexity due to the need for prior data collection and model training.

In contrast, the proposed algorithm adopts a training-free approach and explicitly mitigates EP through the verification process without requiring prior data collection or model training. As summarized in Table 1, the proposed algorithm maintains lower implementation complexity than learning-based approaches. By incorporating a verification process, the proposed algorithm achieves medium–high robustness with medium–low overhead and complexity, providing a balanced solution for practical mmWave WPT systems operating under limited feedback and without prior location information.

III. SYSTEM MODEL AND PROBLEM FORMULATION

In this section, we describe the system model and problem formulation for mmWave WPT systems considered in this paper. The main symbols used in this paper are listed in Table 2.

A. SYSTEM MODEL

As shown in Fig. 1, we consider the mmWave WPT system consisting of the WCS with N_{t} antennas and the WCD with N_{r} antennas. The WCS transmits the RF signals through the mmWave RF module, and the WCD harvests electrical energy from the received signals via its mmWave RF module to power the IoT sensor. The WCS supports L levels of beams, each with a different beamwidth, and selects the transmit beamformer $\mathbf{b}_{\mathrm{t}}$ only from the predefined beam set. The beam set at level l is given by

$$\mathcal{B}_l = \left\{\mathbf{b}_{l,0}, \ldots, \mathbf{b}_{l,N_l-1}\right\}, \tag{1}$$

where $\mathbf{b}_{l,n}$ denotes the n-th beam at level l, and N_l is the total number of beams at level l. The received signal at the WCD is represented as

$$y = \sqrt{P}\mathbf{c}_{\mathrm{r}}^{\mathrm{H}}\mathbf{H}\mathbf{b}_{\mathrm{t}}x + \mathbf{c}_{\mathrm{r}}^{\mathrm{H}}\mathbf{n}, \tag{2}$$

where $\mathbf{H}$ is the mmWave channel matrix, P is the transmit power of the WCS, and x is the transmit signal with unit average power. Here, $\mathbf{c}_{\mathrm{r}}$ is the receive combiner at the WCD, and $\mathbf{n}$ is the additive white Gaussian noise (AWGN) vector with zero mean and variance $\sigma^2\mathbf{I}$. The mmWave channel between the WCS and the WCD is modeled as a sparse scattering channel and can be expressed as

$$\mathbf{H} = \sqrt{\frac{N_{\mathrm{t}}N_{\mathrm{r}}}{N_{\mathrm{p}}}}\sum_{k=1}^{N_{\mathrm{p}}}\alpha_k\mathbf{a}(\phi_k^{\mathrm{r}},\theta_k^{\mathrm{r}})\mathbf{a}(\phi_k^{\mathrm{t}},\theta_k^{\mathrm{t}})^H, \tag{3}$$

where N_{p} denotes the number of multi-paths. For the k-th path, α_k is the complex path gain, ϕ_k^{r} and θ_k^{r} are the azimuth and elevation angles-of-arrival (AoA), respectively, and ϕ_k^{t} and θ_k^{t} are the azimuth and elevation angles-of-departure (AoD), respectively [18]. Here, $\mathbf{a}(\phi,\theta)$ is the array response vector for the uniform planar array (UPA) in the yz-plane, represented as

$$\mathbf{a}(\phi,\theta) = \sqrt{\frac{1}{N}}\Big[1,\ldots,e^{j\frac{2\pi d}{\lambda}(m\sin(\phi)\sin(\theta)+n\cos(\theta))},\ldots,$$
$$\ldots,e^{j\frac{2\pi d}{\lambda}((W-1)\sin(\phi)\sin(\theta)+(H-1)\cos(\theta))}\Big]^T, \tag{4}$$

where λ denotes the wavelength, d is the antenna spacing, $m \in \{0,1,\ldots,W-1\}$ and $n \in \{0,1,\ldots,H-1\}$ are the antenna element indices along the y- and z-axes, respectively, and $N = WH$ is the total number of antenna elements [19].

Based on the linear energy harvesting model in [20], the harvested energy at the WCD is expressed as

$$E = \eta\left|\sqrt{P}\mathbf{c}_{\mathrm{r}}^{\mathrm{H}}\mathbf{H}\mathbf{b}_{\mathrm{t}}x + \mathbf{c}_{\mathrm{r}}^{\mathrm{H}}\mathbf{n}\right|^2, \tag{5}$$

where η is the energy conversion efficiency. Note that while a linear harvesting model is adopted for simplicity, the harvested energy is a monotonically increasing function of the received signal power in practical nonlinear harvesting models [2], [22]. Therefore, maximizing the received signal power also maximizes the harvested energy. As the harvested energy at the WCD strongly depends on the transmit beamformer $\mathbf{b}_{\mathrm{t}}$, the beam selection algorithm plays a critical role in mmWave WPT systems.

B. PROBLEM FORMULATION

We consider the hierarchical beam selection algorithm for the WCS to maximize the harvested energy at the WCD under the predefined beam set constraint. The maximized harvested

energy is obtained by solving the following optimization problem:

$$\max_{\mathbf{b}_\mathrm{t}} E \quad \text{s.t. } \mathbf{b}_\mathrm{t} \in \mathcal{B}_l,\ \forall l, \tag{6}$$

where $\mathcal{B}_l = \{\mathbf{b}_{l,0}, \ldots, \mathbf{b}_{l,N_l-1}\}$ denotes the beam set at level l consisting of N_l discrete beam directions. The receiver combiner $\mathbf{c}_\mathrm{r}$ is set to $\mathbf{b}_{0,0}$, which corresponds to the boresight direction. The optimization problem (6) corresponds to selecting the beam that best aligns with the dominant path between the WCS and the WCD. While the conventional exhaustive search algorithm guarantees optimality, it suffers from high computational complexity [21]. To address this, we propose a hierarchical beam selection algorithm that finds the optimal beam for the WCD while reducing computational complexity. We then implement the proposed algorithm on the commercial mmWave RF module and evaluate its performance in the laboratory environment.

IV. PROPOSED ALGORITHM

In this section, we propose the beam selection algorithm that employs the hierarchical search structure to determine the optimal beam while minimizing computational complexity and mitigating EP. The proposed algorithm consists of the beam identification process and the verification process.

A. BEAM IDENTIFICATION PROCESS

In the beam identification process, the WCS updates the candidate beam set at level l based on the optimal beam selected at level $l+1$. The candidate beam set at level l is expressed as

$$\mathcal{C}_{l,i^\star_{l+1}} = \left\{\mathbf{b}_{l,c} : c \in \mathcal{I}_{l,i^\star_{l+1}}\right\}, \tag{7}$$

where $\mathbf{b}_{l,c}$ represents the beamforming vector corresponding to the c-th beam at level l, and $i^\star_{l+1}$ denotes the optimal beam index at level $l+1$. Here, $\mathcal{I}_{l,i^\star_{l+1}}$ indicates the set of beam indices at level l that spatially overlap with $\mathbf{b}_{l+1,i^\star_{l+1}}$. The structure of the candidate beam set depends on the beamforming architecture of the mmWave RF module. The candidate beam set at level l has a cardinality of $N_{l,c}$.

The WCS sequentially sets the transmit beamformer to $\mathbf{b}_{l,c}$, which is an element of the candidate beam set at level l and collects the corresponding RSSI from the WCD. The RSSI for $\mathbf{b}_{l,c}$ at the WCD is represented as

$$\mathrm{RSSI}_{l,c} = \left\lfloor \left| \sqrt{P}\mathbf{c}_\mathrm{r}^\mathrm{H}\mathbf{H}\mathbf{b}_{l,c}x + \mathbf{c}_\mathrm{r}^\mathrm{H}\mathbf{n} \right|^2 \right\rfloor, \tag{8}$$

where $\lfloor\cdot\rfloor$ denotes the floor function. The optimal beam in the candidate beam set at level l is expressed as

$$\mathbf{b}_{l,c^\star} = \arg \max_{\mathbf{b}_{l,c} \in \mathcal{C}_{l,i^\star_{l+1}}} \left\{\mathrm{RSSI}_{l,c}\right\}. \tag{9}$$

Therefore, the beam that maximizes the RSSI also maximizes the harvested energy under typical energy harvesting models. The selected beam at level l, determined as the optimal one within the candidate beam set, can be incorrect due to various factors, such as multipath reflections in indoor environments and other practical non-ideal effects. Since the optimal beam at level l determines the candidate beam set at level $l-1$, the incorrectly selected beam can cause EP across levels. Practical mmWave WPT systems typically rely on RSSI-based feedback rather than channel state information (CSI), which increases the likelihood of beam selection errors across hierarchical levels. Furthermore, since the harvested energy at the WCD is directly proportional to the received signal power, an incorrectly selected beam directly reduces the harvested energy. To mitigate performance degradation caused by beam selection errors, we introduce the verification process.

B. VERIFICATION PROCESS

In the verification process, the WCS validates the selected beam during the beam identification process. The WCS updates the verification beam set at level l based on the beam with the second-highest RSSI at level $l+1$. The verification beam set at level l is expressed as

$$\mathcal{V}_{l,i^\dagger_{l+1}} \subset \left\{\mathbf{b}_{l,v} : v \in \mathcal{I}_{l,i^\dagger_{l+1}}\right\}, \tag{10}$$

where $\mathbf{b}_{l,v}$ represents the beamforming vector corresponding to the v-th beam at level l, and $i^\dagger_{l+1}$ denotes the beam index with the second-highest RSSI at level $l+1$. Here, $\mathcal{I}_{l,i^\dagger_{l+1}}$ indicates the set of beam indices at level l that spatially overlap with $\mathbf{b}_{l+1,i^\dagger_{l+1}}$. The beam indices in the verification beam set are randomly selected from $\mathcal{I}_{l,i^\dagger_{l+1}}$ to reduce implementation complexity while maintaining sufficient spatial diversity. The verification beam set has a cardinality of $N_{l,v}$, where $N_{l,v} < N_{l,c}$, indicating that the verification beam set is smaller than the candidate beam set.

The WCS sequentially sets the transmit beamformer to $\mathbf{b}_{l,v}$, which is an element of the verification beam set at level l and collects the corresponding RSSI from the WCD to determine the optimal beam in the verification beam set. The optimal beam in the verification beam set at level l is given by

$$\mathbf{b}_{l,v^\star} = \arg \max_{\mathbf{b}_{l,v} \in \mathcal{V}_{l,i^\dagger_{l+1}}} \left\{\mathrm{RSSI}_{l,v}\right\}. \tag{11}$$

Finally, the WCS determines the optimal beam at level l by performing the following operation:

$$\mathbf{b}_{l,i^\star_l} = \arg\max \left\{\mathrm{RSSI}_{l,c^\star},\ \mathrm{RSSI}_{l,v^\star}\right\}, \tag{12}$$

where $i^\star_l$ indicates the beam index with the highest RSSI at level l. In addition, the WCS identifies the beam corresponding to the second-highest RSSI at level l, given by

$$\mathbf{b}_{l,i^\dagger_l} = \arg \max_{\mathbf{b}_{l,k} \in \left(\mathcal{C}_{l,i^\star_{l+1}} \cup \mathcal{V}_{l,i^\dagger_{l+1}}\right) \setminus \left\{\mathbf{b}_{l,i^\star_l}\right\}} \left\{\mathrm{RSSI}_{l,k}\right\}, \tag{13}$$

where $\mathrm{RSSI}_{l,k}$ represents the RSSI associated with $\mathbf{b}_{l,k}$ in the union of the candidate beam and the verification beam sets, and $i^\dagger_l$ indicates the beam index with the second-highest RSSI

Algorithm 1 Proposed Algorithm

Initialize $i^{\star}_{L+1} = 0$ and $\mathcal{I}_{L,i^{\star}_{L+1}} = \{1, \ldots, N_L\}$
for $l = L, L-1, \cdots, 1$ **do**
  Update candidate beam set, $\mathcal{C}_{l,i^{\star}_{l+1}}$
  for $\forall \mathbf{b}_{l,c} \in \mathcal{C}_{l,i^{\star}_{l+1}}$ **do**
    Set transmit beamformer to $\mathbf{b}_{l,c}$
    Collect RSSI for beam $\mathbf{b}_{l,c}$
  end for
  Select optimal beam $\mathbf{b}_{l,c^{\star}}$ in candidate beam set
  Update verification beam set, $\mathcal{V}_{l,i^{\dagger}_{l+1}}$
  for $\forall \mathbf{b}_{l,v} \in \mathcal{V}_{l,i^{\dagger}_{l+1}}$ **do**
    Set transmit beamformer to $\mathbf{b}_{l,v}$
    Collect RSSI for beam $\mathbf{b}_{l,v}$
  end for
  Select optimal beam $\mathbf{b}_{l,v^{\star}}$ in validation beam set
  Determine optimal beam at level l, $\mathbf{b}_{l,i^{\star}_{l}}$
  Compute beam with second-highest RSSI at level l, $\mathbf{b}_{l,i^{\dagger}_{l}}$
end for

TABLE 3. Computational complexity of three algorithms.

Exhaustive Search	Conventional	Proposed
$\mathcal{O}(N_1)$	$\mathcal{O}\left(\sum_{l=1}^{L} N_{l,c}\right)$	$\mathcal{O}\left(\sum_{l=1}^{L}(N_{l,c}+N_{l,v})\right)$

at level l. The beam $\mathbf{b}_{l,i^{\dagger}_{l}}$ is used to construct the verification beam set employed in the verification process at level $l-1$. The beam identification and the verification processes are sequentially performed from $l = L$ down to $l = 1$, where L denotes the total number of hierarchical levels supported by the WCS, with lower levels having narrower beamwidths to enable stepwise beam selection. The benefit of the verification step is maximized when the RSSI difference between the highest and second-highest beams at the upper level is small, which typically occurs in indoor environments where multipath reflections from surrounding objects cause ambiguity in beam selection. The overall procedure of the proposed algorithm is summarized in Algorithm 1. A flowchart illustrating the hierarchical beam selection procedure is shown in Fig. 2 for better clarity.

C. COMPLEXITY ANALYSIS

The computational complexity of the proposed algorithms is determined by the number of beam allocations required to identify the optimal beam. We analyze the computational complexity of three algorithms: *Exhaustive*, *Conventional*, and *Proposed*. *Exhaustive* determines the optimal beam using the exhaustive search algorithm. *Conventional* conducts hierarchical beam selection without the verification process, whereas *Proposed* integrates the verification process into hierarchical beam selection.

The proposed algorithm utilizes $N_{l,c}$ candidate beams and $N_{l,v}$ verification beams at each level l, resulting in the overall computational complexity of $\mathcal{O}\left(\sum_{l=1}^{L}(N_{l,c}+N_{l,v})\right)$. In contrast, the conventional algorithm in [12], [13] employs hierarchical beamforming without the verification process, resulting in a lower complexity of $\mathcal{O}\left(\sum_{l=1}^{L} N_{l,c}\right)$. The exhaustive search algorithm evaluates all N_1 beams with the narrowest beamwidth at level 1, resulting in a highest complexity of $\mathcal{O}(N_1)$. The computational complexity of three algorithms is summarized in Table 3.

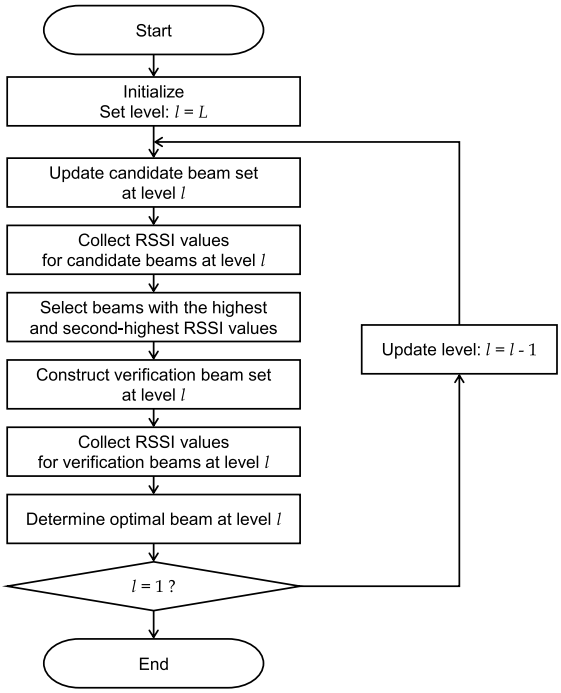

FIGURE 2. Flowchart of the proposed hierarchical beam selection algorithm including the verification process.

In general, the number of all beams with the narrowest beamwidth at level 1, denoted by N_1, satisfies the inequality

$$N_1 \gg \sum_{l=1}^{L}(N_{l,c}+N_{l,v}). \tag{14}$$

The inequality in (14) implies that the proposed algorithm achieves lower computational complexity than the exhaustive search algorithm. Although the computational complexity of the proposed algorithm is slightly higher than the conventional algorithm due to the additional verification process, this overhead is essential to mitigate EP across levels.

V. IMPLEMENTATION ON COMMERCIAL mmWave RF MODULE

In this section, we present the implementation of the proposed algorithm on the commercial mmWave RF module to evaluate its performance in the laboratory environment.

A. COMMERCIAL mmWave RF MODULE

Fig. 3 shows the commercial mmWave RF module used to validate the proposed algorithm [23]. The mmWave RF

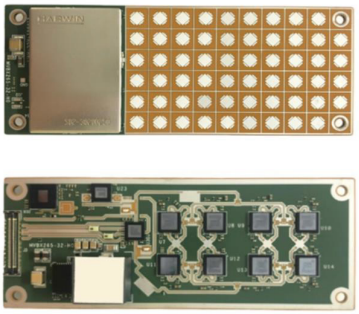

FIGURE 3. Commercial mmWave RF module.

TABLE 4. Commercial mmWave RF module specifications.

Parameter	Value
Frequency range	24.25–27.5 GHz
Number of levels	3
Number of beams per level	58 (level 1), 17 (level 2), 9 (level 3)
Beam scan range	±60° (Azimuth/Elevation)
Intermediate frequency	4.4–5.6 GHz
EIRP	38 dBm
Gain	42 dB (Receive mode)

module operates within the 24.25–27.5 GHz frequency range and supports the maximum effective isotropic radiated power (EIRP) of 38 dBm. It can be configured for either transmit or receive mode. The mmWave RF module supports three levels of beams, each with a different beamwidth, specified as 30° × 15° for level 1, 30° × 30° for level 2, and 60° × 15° for level 3, corresponding to horizontal and vertical directions, respectively. Note that lower levels correspond to narrower beamwidths, allowing for finer resolution in beam selection. Table 4 summarizes the key specifications of the mmWave RF module used in our implementation.

Figs. 4(a), 4(b), and 4(c) illustrate the hierarchical beamforming structure of the mmWave RF module across three levels. Specifically, Fig. 4(a) presents the beam indices and the corresponding radiation directions at level 1, where $\mathbf{b}_{1,0}$ corresponds to the front direction, $\mathbf{b}_{1,7}$ to the left, $\mathbf{b}_{1,13}$ to the right, $\mathbf{b}_{1,10}$ to the top, and $\mathbf{b}_{1,16}$ to the bottom, respectively. It is important to note that the optimal beam at the WCS dynamically changes depending on the relative spatial position of the WCD.

As the beam level decreases, the mmWave RF module employs narrower beamwidths, resulting in a larger number of configurable beam indices at lower levels in the WCS, as shown in Figs. 4(a), 4(b), and 4(c). Therefore, hierarchical beam selection from higher to lower levels reduces the overall computational complexity.

B. CONSTRUCTION OF CANDIDATE BEAM SETS

To implement the proposed algorithm on the commercial mmWave RF module, the candidate beam set at each level is constructed based on the predefined beam set. Specifically, the

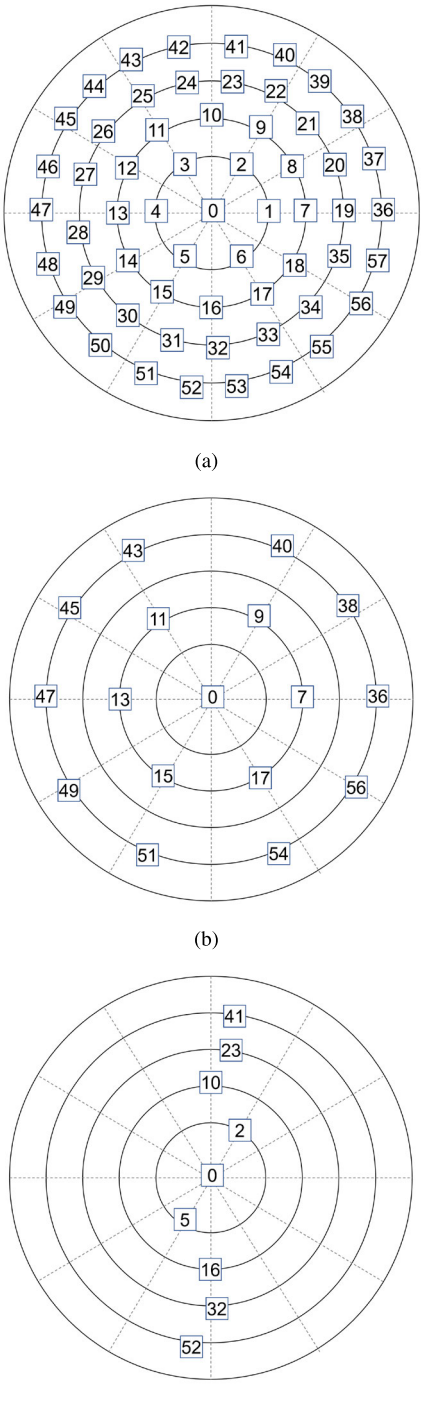

FIGURE 4. Beam index at level(a) $l = 1$,(b) $l = 2$, and(c) $l = 3$.

candidate beams at level l are selected such that their radiation patterns spatially overlap with the optimal beam at level $l + 1$.

As shown in Fig. 4(c), the candidate beam set at level 3 is defined as

$$\mathcal{C}_{3,0} = \left\{\mathbf{b}_{3,0},\ \mathbf{b}_{3,10},\ \mathbf{b}_{3,16},\ \mathbf{b}_{3,23},\ \mathbf{b}_{3,32},\ \mathbf{b}_{3,41},\ \mathbf{b}_{3,52}\right\}. \tag{15}$$

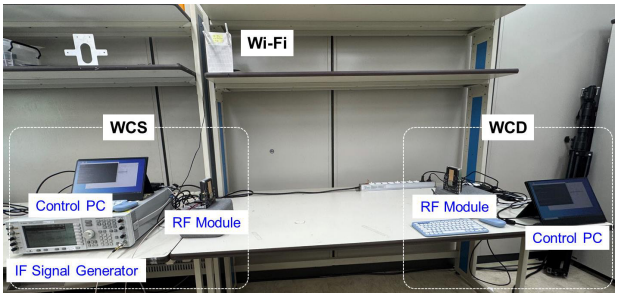

FIGURE 5. Experimental setup.

Here, $\mathbf{b}_{3,2}$ and $\mathbf{b}_{3,5}$, which do not spatially overlap with beams at level 2, are excluded from the candidate beam set at level 3 to reduce the number of beam allocations.

As illustrated in Figs. 4(b) and 4(c), the candidate beam sets at level 2 are determined based on the optimal beam at level 3. For example, when $\mathbf{b}_{3,0}$ is selected as the optimal beam at level 3, the candidate beam set at level 2 is expressed as

$$\mathcal{C}_{2,0} = \left\{\mathbf{b}_{2,47},\ \mathbf{b}_{2,13},\ \mathbf{b}_{2,0},\ \mathbf{b}_{2,7},\ \mathbf{b}_{2,36}\right\}. \tag{16}$$

Similarly, the candidate beam set at level 1 is obtained based on the optimal beam at level 2, as shown in Figs. 4(a) and 4(b). For example, when $\mathbf{b}_{2,47}$ is chosen as the optimal beam at level 2, the candidate beam set at level 1 is expressed as

$$\mathcal{C}_{1,47} = \left\{\mathbf{b}_{1,47},\ \mathbf{b}_{1,48},\ \mathbf{b}_{1,29},\ \mathbf{b}_{1,28},\ \mathbf{b}_{1,27},\ \mathbf{b}_{1,46}\right\}. \tag{17}$$

The candidate beam sets for all levels are summarized in Table 5. It is worth noting that the construction of the candidate beam set may vary depending on the beamforming structure of the mmWave RF module.

VI. EXPERIMENTAL VALIDATION OF PROPOSED ALGORITHM

In this section, we experimentally validate the performance of the proposed algorithm using the commercial mmWave RF module in the laboratory environment.

A. EXPERIMENTAL SETUP

Fig. 5 shows the experimental setup, which consists of the WCS, the WCD, and the Wi-Fi access point (AP). The WCS is composed of the mmWave RF module operating in transmit mode, the intermediate frequency (IF) signal generator, and the control PC. In the WCS, the continuous-wave (CW) signal with a carrier frequency 26 GHz is used for mmWave WPT. The mmWave RF module upconverts a 5 GHz CW IF signal generated by the signal generator, and the EIRP is set to 20 dBm. The control PC manages the operation of the mmWave RF module and requests the RSSI[1] from the WCD. The WCD consists of the mmWave RF module operating in receive mode and the control PC. In the WCD, the mmWave RF module is configured to receive the 26 GHz CW signal, providing a receive gain of 42 dB. The receive combiner is set to $\mathbf{c}_{\mathrm{r}} = \mathbf{b}_{1,0}$. The control PC measures the RSSI at the mmWave RF module and feeds it back to the WCS. The WCS and the WCD communicate over Wi-Fi using the user datagram protocol (UDP) to exchange messages related to the operation of the proposed algorithm, such as RSSI requests and responses.

The experiments were conducted in an indoor laboratory environment, representing typical mmWave WPT deployment scenarios. While the setup was LoS-dominant, natural multipath reflections from surrounding walls and objects were present, and no artificial reflectors were introduced. Channel parameters such as RMS delay spread and K-factor were not explicitly measured, as the focus of the experiments was on evaluating the proposed algorithm under practical indoor conditions using RSSI-based measurements.

In our experiment, the position of the WCS is fixed, while the WCD is moved to evaluate the robustness and effectiveness of the proposed algorithm. We consider three deployment scenarios. In Scenario 1, the WCD is located along the boresight direction of the WCS, corresponding to an azimuth angle of 0° and an elevation angle of 0°. In Scenario 2, the WCD is positioned at an azimuth angle of 44° and an elevation angle of 10° relative to the WCS boresight. In Scenario 3, the WCD moves among five fixed locations with different angular positions relative to the WCS boresight. In all scenarios, the distance between the WCS and the WCD is fixed at 2 meters. For all levels, the cardinality of the verification beam set is configured as $N_{l,v} = 2$.

B. EXPERIMENTAL RESULTS

Figs. 6 and 7 show the execution log of the proposed algorithm implemented in the WCS and the WCD under Scenario 1. The WCS sequentially allocates the transmit beamformer from the candidate beam set at level 3, defined as

$$\mathcal{C}_{3,0} = \left\{\mathbf{b}_{3,0},\ \mathbf{b}_{3,10},\ \mathbf{b}_{3,16},\ \mathbf{b}_{3,23},\ \mathbf{b}_{3,32},\ \mathbf{b}_{3,41},\ \mathbf{b}_{3,52}\right\}, \tag{18}$$

and collects the RSSI values measured at the WCD. Since the WCD is located directly in front of the WCS, $\mathbf{b}_{3,0}$ achieves the highest RSSI of 1058, and $\mathbf{b}_{3,32}$ achieves the second-highest RSSI of 121.

The candidate beam set at level 2 associated with $\mathbf{b}_{3,0}$ is given by

$$\mathcal{C}_{2,0} = \left\{\mathbf{b}_{2,47},\ \mathbf{b}_{2,13},\ \mathbf{b}_{2,0},\ \mathbf{b}_{2,7},\ \mathbf{b}_{2,36}\right\}. \tag{19}$$

Based on the RSSI values measured at the WCD, the WCS selects $\mathbf{b}_{2,0}$ which provides the highest RSSI of 986. It is worth noting that $\mathbf{b}_{2,47}$, $\mathbf{b}_{2,13}$ and $\mathbf{b}_{2,7}$ show relatively high RSSI due to signal reflections from surrounding walls. To verify the selected beam, the WCS assigns the transmit beamformer from the verification beam set at level 2, given by

$$\mathcal{V}_{2,32} = \left\{\mathbf{b}_{2,56},\ \mathbf{b}_{2,49}\right\}. \tag{20}$$

[1]The RSSI is a digital value derived from the analog output of the power detector in the mmWave RF module, and it is internally quantized by the analog-to-digital converter (ADC). The reported values are relative and unitless, depending on the implementation of the mmWave RF module.

TABLE 5. Candidate beam sets for all levels.

Level	Optimal Beam at Upper Level	Candidate Beam Set	Beam Elements
3	–	$\mathcal{C}_{3,0}$	$\{\mathbf{b}_{3,0},\ \mathbf{b}_{3,10},\ \mathbf{b}_{3,16},\ \mathbf{b}_{3,23},\ \mathbf{b}_{3,32},\ \mathbf{b}_{3,41},\ \mathbf{b}_{3,52}\}$
2	$\mathbf{b}_{3,0}$	$\mathcal{C}_{2,0}$	$\{\mathbf{b}_{2,47},\ \mathbf{b}_{2,13},\ \mathbf{b}_{2,0},\ \mathbf{b}_{2,7},\ \mathbf{b}_{2,36}\}$
	$\mathbf{b}_{3,10}$	$\mathcal{C}_{2,10}$	$\{\mathbf{b}_{2,11},\ \mathbf{b}_{2,9}\}$
	$\mathbf{b}_{3,16}$	$\mathcal{C}_{2,16}$	$\{\mathbf{b}_{2,15},\ \mathbf{b}_{2,17}\}$
	$\mathbf{b}_{3,23}$	$\mathcal{C}_{2,23}$	$\{\mathbf{b}_{2,45},\ \mathbf{b}_{2,38}\}$
	$\mathbf{b}_{3,32}$	$\mathcal{C}_{2,32}$	$\{\mathbf{b}_{2,49},\ \mathbf{b}_{2,56}\}$
	$\mathbf{b}_{3,41}$	$\mathcal{C}_{2,41}$	$\{\mathbf{b}_{2,43},\ \mathbf{b}_{2,40}\}$
	$\mathbf{b}_{3,52}$	$\mathcal{C}_{2,52}$	$\{\mathbf{b}_{2,51},\ \mathbf{b}_{2,54}\}$
1	$\mathbf{b}_{2,0}$	$\mathcal{C}_{1,0}$	$\{\mathbf{b}_{1,0},\ \mathbf{b}_{1,1},\ \mathbf{b}_{1,2},\ \mathbf{b}_{1,3},\ \mathbf{b}_{1,4},\ \mathbf{b}_{1,5},\ \mathbf{b}_{1,6}\}$
	$\mathbf{b}_{2,7}$	$\mathcal{C}_{1,7}$	$\{\mathbf{b}_{1,7},\ \mathbf{b}_{1,1},\ \mathbf{b}_{1,8},\ \mathbf{b}_{1,20},\ \mathbf{b}_{1,19},\ \mathbf{b}_{1,35},\ \mathbf{b}_{1,18}\}$
	$\mathbf{b}_{2,9}$	$\mathcal{C}_{1,9}$	$\{\mathbf{b}_{1,9},\ \mathbf{b}_{1,2},\ \mathbf{b}_{1,8},\ \mathbf{b}_{1,21},\ \mathbf{b}_{1,22},\ \mathbf{b}_{1,23},\ \mathbf{b}_{1,10}\}$
	$\mathbf{b}_{2,11}$	$\mathcal{C}_{1,11}$	$\{\mathbf{b}_{1,11},\ \mathbf{b}_{1,3},\ \mathbf{b}_{1,10},\ \mathbf{b}_{1,24},\ \mathbf{b}_{1,35},\ \mathbf{b}_{1,26},\ \mathbf{b}_{1,12}\}$
	$\mathbf{b}_{2,13}$	$\mathcal{C}_{1,13}$	$\{\mathbf{b}_{1,13},\ \mathbf{b}_{1,4},\ \mathbf{b}_{1,12},\ \mathbf{b}_{1,27},\ \mathbf{b}_{1,28},\ \mathbf{b}_{1,29},\ \mathbf{b}_{1,14}\}$
	$\mathbf{b}_{2,15}$	$\mathcal{C}_{1,15}$	$\{\mathbf{b}_{1,15},\ \mathbf{b}_{1,5},\ \mathbf{b}_{1,14},\ \mathbf{b}_{1,29},\ \mathbf{b}_{1,30},\ \mathbf{b}_{1,31},\ \mathbf{b}_{1,16}\}$
	$\mathbf{b}_{2,17}$	$\mathcal{C}_{1,17}$	$\{\mathbf{b}_{1,17},\ \mathbf{b}_{1,6},\ \mathbf{b}_{1,16},\ \mathbf{b}_{1,32},\ \mathbf{b}_{1,33},\ \mathbf{b}_{1,34},\ \mathbf{b}_{1,18}\}$
	$\mathbf{b}_{2,36}$	$\mathcal{C}_{1,36}$	$\{\mathbf{b}_{1,36},\ \mathbf{b}_{1,37},\ \mathbf{b}_{1,20},\ \mathbf{b}_{1,19},\ \mathbf{b}_{1,35},\ \mathbf{b}_{1,57}\}$
	$\mathbf{b}_{2,38}$	$\mathcal{C}_{1,38}$	$\{\mathbf{b}_{1,38},\ \mathbf{b}_{1,37},\ \mathbf{b}_{1,20},\ \mathbf{b}_{1,21},\ \mathbf{b}_{1,22},\ \mathbf{b}_{1,39}\}$
	$\mathbf{b}_{2,40}$	$\mathcal{C}_{1,40}$	$\{\mathbf{b}_{1,40},\ \mathbf{b}_{1,39},\ \mathbf{b}_{1,21},\ \mathbf{b}_{1,22},\ \mathbf{b}_{1,23},\ \mathbf{b}_{1,41}\}$
	$\mathbf{b}_{2,43}$	$\mathcal{C}_{1,43}$	$\{\mathbf{b}_{1,43},\ \mathbf{b}_{1,44},\ \mathbf{b}_{1,26},\ \mathbf{b}_{1,25},\ \mathbf{b}_{1,24},\ \mathbf{b}_{1,42}\}$
	$\mathbf{b}_{2,45}$	$\mathcal{C}_{1,45}$	$\{\mathbf{b}_{1,45},\ \mathbf{b}_{1,46},\ \mathbf{b}_{1,27},\ \mathbf{b}_{1,26},\ \mathbf{b}_{1,25},\ \mathbf{b}_{1,44}\}$
	$\mathbf{b}_{2,47}$	$\mathcal{C}_{1,47}$	$\{\mathbf{b}_{1,47},\ \mathbf{b}_{1,48},\ \mathbf{b}_{1,29},\ \mathbf{b}_{1,28},\ \mathbf{b}_{1,27},\ \mathbf{b}_{1,46}\}$
	$\mathbf{b}_{2,49}$	$\mathcal{C}_{1,49}$	$\{\mathbf{b}_{1,49},\ \mathbf{b}_{1,50},\ \mathbf{b}_{1,30},\ \mathbf{b}_{1,29},\ \mathbf{b}_{1,28},\ \mathbf{b}_{1,48}\}$
	$\mathbf{b}_{2,51}$	$\mathcal{C}_{1,51}$	$\{\mathbf{b}_{1,51},\ \mathbf{b}_{1,52},\ \mathbf{b}_{1,32},\ \mathbf{b}_{1,31},\ \mathbf{b}_{1,30},\ \mathbf{b}_{1,50}\}$
	$\mathbf{b}_{2,54}$	$\mathcal{C}_{1,54}$	$\{\mathbf{b}_{1,54},\ \mathbf{b}_{1,55},\ \mathbf{b}_{1,34},\ \mathbf{b}_{1,33},\ \mathbf{b}_{1,32},\ \mathbf{b}_{1,53}\}$
	$\mathbf{b}_{2,56}$	$\mathcal{C}_{1,56}$	$\{\mathbf{b}_{1,56},\ \mathbf{b}_{1,57},\ \mathbf{b}_{1,19},\ \mathbf{b}_{1,35},\ \mathbf{b}_{1,34},\ \mathbf{b}_{1,55}\}$

Since the RSSI values of the verification beams at level 2 are lower than that of $\mathbf{b}_{2,0}$, the WCS maintains $\mathbf{b}_{2,0}$ as the optimal beam at level 2. In addition, the WCS identifies $\mathbf{b}_{2,13}$ as the beam with the second-highest RSSI to construct the verification beam set at level 1.

The candidate beam set at level 1 associated with $\mathbf{b}_{2,0}$ is given by

$$\mathcal{C}_{1,0} = \left\{\mathbf{b}_{1,0},\ \mathbf{b}_{1,1},\ \mathbf{b}_{1,2},\ \mathbf{b}_{1,3},\ \mathbf{b}_{1,4},\ \mathbf{b}_{1,5},\ \mathbf{b}_{1,6}\right\}. \quad (21)$$

According to the RSSI values measured at the WCD, the WCS selects $\mathbf{b}_{1,0}$ as the optimal beam with the highest RSSI of 1002. The verification beam set at level 1 associated with $\mathbf{b}_{2,13}$ is chosen as

$$\mathcal{V}_{1,13} = \left\{\mathbf{b}_{1,27},\ \mathbf{b}_{1,13}\right\}. \quad (22)$$

Since the RSSI values of the verification beams are lower than that of $\mathbf{b}_{1,0}$, the WCS confirms $\mathbf{b}_{1,0}$ as the final optimal beam at level 1.

In Scenario 1, the WCD is located along the boresight direction of the WCS, corresponding to an azimuth angle of 0° and an elevation angle of 0°. The exhaustive search algorithm, which evaluates 58 candidate beams, identifies $\mathbf{b}_{1,0}$ as the global optimal beam. The proposed algorithm converges to the same global optimum using only 23 beam allocations, resulting in a 60 % reduction in computational complexity compared to exhaustive search.

Fig. 7 shows the operation of the WCD, where the RSSI is measured from the received RF signals and reported to the WCS. Table 6 summarizes the experimental results for Scenario 1.

TABLE 6. Experimental results for Scenario 1.

level 3		level 2		level 1	
Beam	RSSI	Beam	RSSI	Beam	RSSI
0	**1058**	47	294	**0**	**1002**
10	119	13	382	1	830
16	117	**0**	**986**	2	550
23	119	7	298	3	489
32	121	36	158	4	862
41	117	56	223	5	738
52	119	49	146	6	599
-	-	-	-	27	602
-	-	-	-	13	570

Figs. 8 and 9 show the execution log of the proposed algorithm implemented in the WCS and the WCD under Scenario 2. The WCS allocates the transmit beamformer from the candidate beam set at level 3, defined as

$$\mathcal{C}_{3,0} = \left\{\mathbf{b}_{3,0},\ \mathbf{b}_{3,10},\ \mathbf{b}_{3,16},\ \mathbf{b}_{3,23},\ \mathbf{b}_{3,32},\ \mathbf{b}_{3,41},\ \mathbf{b}_{3,52}\right\}, \quad (23)$$

and collects the RSSI values measured at the WCD. Here, $\mathbf{b}_{3,52}$ and $\mathbf{b}_{3,0}$ achieve the highest RSSI of 129 and the second-highest RSSI of 125 at the WCD, respectively. Although $\mathbf{b}_{3,52}$ is directed toward the bottom as shown in Fig. 4(c), the WCS selects $\mathbf{b}_{3,52}$ as the optimal beam at level 3. The beam $\mathbf{b}_{3,52}$ temporarily achieves the highest RSSI at level 3 due to channel reflections off the floor, which can lead to EP at level 2.

The candidate beam set at level 2 associated with $\mathbf{b}_{3,52}$ is given by

$$\mathcal{C}_{2,52} = \left\{\mathbf{b}_{2,51},\ \mathbf{b}_{2,54}\right\}. \quad (24)$$

```
[Initialization]

[Level 3]
Beam Selection Process
> Update candidate beam index: [0, 10, 16, 23, 32, 41, 52]
- Set b_3,0  -> request RSSI from WCD
- Set b_3,10 -> request RSSI from WCD
- Set b_3,16 -> request RSSI from WCD
- Set b_3,23 -> request RSSI from WCD
- Set b_3,32 -> request RSSI from WCD
- Set b_3,41 -> request RSSI from WCD
- Set b_3,52 -> request RSSI from WCD
- RSSI values [1058, 119, 117, 119, 121, 117, 119]
- Highest RSSI beam in candidate beams: b_3,0

* Optimal beam: b_3,0
* Second-highest RSSI beam: b_3,32

[Level 2]
Beam Selection Process
> Update candidate beam index: [47, 13, 0, 7, 36]
- Set b_2,47 -> request RSSI from WCD
- Set b_2,13 -> request RSSI from WCD
- Set b_2,0  -> request RSSI from WCD
- Set b_2,7  -> request RSSI from WCD
- Set b_2,36 -> request RSSI from WCD
- RSSI values [294, 382, 986, 298, 158]
- Highest RSSI beam in candidate beams: b_2,0

Verification Process
> Update verification beam index: [56, 49]
- Set b_2,56 -> request RSSI from WCD
- Set b_2,49 -> request RSSI from WCD
- RSSI values [146, 174]
- Highest RSSI beam in verification beams: b_2,49

* Optimal beam: b_2,0
* Second-highest RSSI beam: b_2,13

[Level 1]
Beam Selection Process
> Update candidate beam index: [0, 1, 2, 3, 4, 5, 6]
- Set b_1,0 -> request RSSI from WCD
- Set b_1,1 -> request RSSI from WCD
- Set b_1,2 -> request RSSI from WCD
- Set b_1,3 -> request RSSI from WCD
- Set b_1,4 -> request RSSI from WCD
- Set b_1,5 -> request RSSI from WCD
- Set b_1,6 -> request RSSI from WCD
- RSSI values [1002, 830, 550, 489, 862, 738, 599]
- Highest RSSI beam in candidate beams: b_1,0

Verification Process
> Update verification beam set: [27, 13]
- Set b_1,27 -> request RSSI from WCD
- Set b_1,13 -> request RSSI from WCD
- RSSI values [602, 570]
- Highest RSSI beam in verification beams: b_1,27

* Optimal beam: b_1,0
-----------------------------------------------------
Final optimal beam for WCD: b_1,0
-----------------------------------------------------
```

FIGURE 6. Execution log of proposed algorithm implemented in WCS under Scenario 1, showing beam identification and verification processes across levels.

Based on the RSSI values measured at the WCD, the WCS selects $\mathbf{b}_{2,51}$ as the optimal beam with the highest RSSI of 194. Subsequently, the WCS allocates the transmit beamformer from the verification beam set and collects the RSSI measured at the WCD to verify the selected beam. The verification beam set at level 2 associated with $\mathbf{b}_{3,0}$ is chosen as

$$\mathcal{V}_{2,0} = \left\{\mathbf{b}_{2,47},\ \mathbf{b}_{2,7}\right\}. \tag{25}$$

```
*******************************************
- Measure RSSI = 1058 -> Report to WCS
- Measure RSSI = 119 -> Report to WCS
- Measure RSSI = 117 -> Report to WCS
- Measure RSSI = 119 -> Report to WCS
- Measure RSSI = 121 -> Report to WCS
- Measure RSSI = 117 -> Report to WCS
- Measure RSSI = 119 -> Report to WCS
- Measure RSSI = 294 -> Report to WCS
- Measure RSSI = 382 -> Report to WCS
- Measure RSSI = 986 -> Report to WCS
- Measure RSSI = 298 -> Report to WCS
- Measure RSSI = 158 -> Report to WCS
- Measure RSSI = 146 -> Report to WCS
- Measure RSSI = 174 -> Report to WCS
- Measure RSSI = 1002 -> Report to WCS
- Measure RSSI = 830 -> Report to WCS
- Measure RSSI = 550 -> Report to WCS
- Measure RSSI = 489 -> Report to WCS
- Measure RSSI = 862 -> Report to WCS
- Measure RSSI = 738 -> Report to WCS
- Measure RSSI = 599 -> Report to WCS
- Measure RSSI = 602 -> Report to WCS
- Measure RSSI = 570 -> Report to WCS
*******************************************
```

FIGURE 7. Execution log of proposed algorithm implemented in WCD under Scenario 1, showing measured RSSI and reporting it to the WCS.

Since $\mathbf{b}_{2,47}$ in the verification beam set achieves a higher RSSI of 521 compared to 194 for $\mathbf{b}_{2,51}$ in the candidate beam set, the WCS updates $\mathbf{b}_{2,47}$ as the optimal beam at level 2. In addition, the WCS identifies $\mathbf{b}_{2,51}$ as the beam with the second-highest RSSI to construct the verification beam set at level 1.

The candidate beam set at level 1 associated with $\mathbf{b}_{2,51}$ is given by

$$\mathcal{C}_{1,47} = \left\{\mathbf{b}_{1,47},\ \mathbf{b}_{1,48},\ \mathbf{b}_{1,29},\ \mathbf{b}_{1,28},\ \mathbf{b}_{1,27},\ \mathbf{b}_{1,46}\right\}. \tag{26}$$

According to the RSSI values measured at the WCD, the WCS selects $\mathbf{b}_{1,46}$ as the optimal beam with the highest RSSI of 1242. The verification beam set at level 1 associated with $\mathbf{b}_{2,51}$ is chosen as

$$\mathcal{V}_{1,51} = \left\{\mathbf{b}_{1,52},\ \mathbf{b}_{1,31}\right\}. \tag{27}$$

Since the RSSI values of the verification beams are lower than that of $\mathbf{b}_{1,46}$, the WCS confirms $\mathbf{b}_{1,46}$ as the final optimal beam at level 1,

In Scenario 2, the WCD is positioned at an azimuth angle of 44° and an elevation angle of 10° relative to the WCS boresight. The exhaustive search algorithm, which evaluates 58 candidate beams, identifies $\mathbf{b}_{1,46}$ as the global optimal beam. The proposed algorithm converges to the same global optimum using only 19 beam allocations, achieving a 67 % reduction in computational complexity compared to the exhaustive search. The verification process prevents EP at level 2.

Fig. 9 shows the operation of the WCD, where the RSSI is measured from the received RF signals and reported to the WCS. Table 7 summarizes the experimental results for Scenario 2.

Figs. 10, 11, and 12 show the averaged experimental results for Scenario 3. Each data point in Figs. 10, 11, and 12 was obtained by averaging five repeated RSSI measurements conducted at each of the five fixed WCD locations.

```
[Initialization]

[Level 3]
Beam Selection Process
> Update candidate beam index: [0, 10, 16, 23, 32, 41, 52]
- Set b_3,0  -> request RSSI from WCD
- Set b_3,10 -> request RSSI from WCD
- Set b_3,16 -> request RSSI from WCD
- Set b_3,23 -> request RSSI from WCD
- Set b_3,32 -> request RSSI from WCD
- Set b_3,41 -> request RSSI from WCD
- Set b_3,52 -> request RSSI from WCD
- RSSI values [125, 114, 114, 114, 114, 114, 129]
- Highest RSSI beam in candidate beams: b_3,52

* Optimal beam: b_3,52
* Second-highest RSSI beam: b_3,0

[Level 2]
Beam Selection Process
> Update candidate beam index: [51, 54]
- Set b_2,51 -> request RSSI from WCD
- Set b_2,54 -> request RSSI from WCD
- RSSI values [194, 114]
- Highest RSSI beam in candidate beams: b_2,51

Verification Process
> Update verification beam index: [47, 7]
- Set b_2,47 -> request RSSI from WCD
- Set b_2,7 -> request RSSI from WCD
- RSSI values [521, 118]
- Highest RSSI beam in verification beams: b_2,47

* Optimal beam: b_2,47
* Second-highest RSSI beam: b_2,51

[Level 1]
Beam Selection Process
> Update candidate beam index: [47, 48, 29, 28, 27, 46]
- Set b_1,47 -> request RSSI from WCD
- Set b_1,48 -> request RSSI from WCD
- Set b_1,29 -> request RSSI from WCD
- Set b_1,28 -> request RSSI from WCD
- Set b_1,27 -> request RSSI from WCD
- Set b_1,46 -> request RSSI from WCD
- RSSI values [537, 346, 361, 117, 1185, 1242]
- Highest RSSI beam in candidate beams: b_1,46

Verification Process
> Update verification beam set: [52, 31]
- Set b_1,52 -> request RSSI from WCD
- Set b_1,31 -> request RSSI from WCD
- RSSI values [117, 120]
- Highest RSSI beam in verification beams: b_1,31

* Optimal beam: b_1,46
------------------------------------------------------
Final optimal beam for WCD: b_1,46
------------------------------------------------------
```

FIGURE 8. Execution log of proposed algorithm implemented in WCS under Scenario 2, highlighting EP mitigation via verification process.

```
**********************************************
- Measure RSSI = 125 -> Report to WCS
- Measure RSSI = 114 -> Report to WCS
- Measure RSSI = 114 -> Report to WCS
- Measure RSSI = 114 -> Report to WCS
- Measure RSSI = 114 -> Report to WCS
- Measure RSSI = 114 -> Report to WCS
- Measure RSSI = 129 -> Report to WCS
- Measure RSSI = 194 -> Report to WCS
- Measure RSSI = 114 -> Report to WCS
- Measure RSSI = 521 -> Report to WCS
- Measure RSSI = 118 -> Report to WCS
- Measure RSSI = 537 -> Report to WCS
- Measure RSSI = 346 -> Report to WCS
- Measure RSSI = 361 -> Report to WCS
- Measure RSSI = 117 -> Report to WCS
- Measure RSSI = 1185 -> Report to WCS
- Measure RSSI = 1242 -> Report to WCS
- Measure RSSI = 117 -> Report to WCS
- Measure RSSI = 120 -> Report to WCS
**********************************************
```

FIGURE 9. Execution log of proposed algorithm implemented in WCD under Scenario 2, showing measured RSSI and reporting it to the WCS.

TABLE 7. Experimental results for Scenario 2.

level 3		level 2		level 1	
Beam	**RSSI**	**Beam**	**RSSI**	**Beam**	**RSSI**
0	125	51	194	47	537
10	114	54	114	48	346
16	114	**47**	**521**	29	361
23	114	7	118	28	117
32	114	-	-	27	1185
41	114	-	-	**46**	**1242**
52	**129**	-	-	52	117
-	-	-	-	31	120

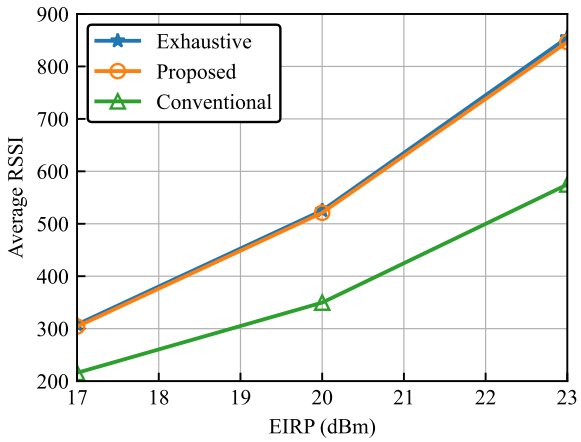

FIGURE 10. Average RSSI versus EIRP at WCS for Scenario 3.

Figs. 10 and 11 present the average RSSI measured at the WCD and the average number of beam allocations, respectively, for various EIRP values transmitted by the WCS in Scenario 3. To evaluate the performance of the proposed algorithm, we compare three algorithms: *Exhaustive*, *Conventional*, and *Proposed*. It is observed that the proposed algorithm achieves near-optimal RSSI performance while requiring, on average, 40 % of beam allocations compared to the exhaustive search algorithm. It is also observed that the proposed algorithm improves the average RSSI performance by approximately 40 % compared to the conventional algorithm while incurring only a 20 % increase in the number of beam allocation. We confirm that the verification process in the proposed algorithm mitigates EP across levels

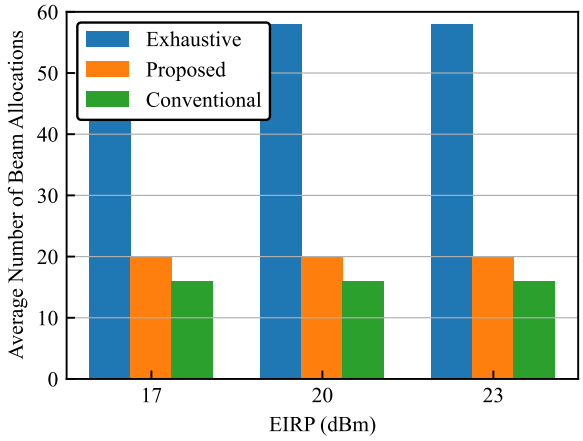

FIGURE 11. Average number of beam allocations versus EIRP at WCS for Scenario 3.

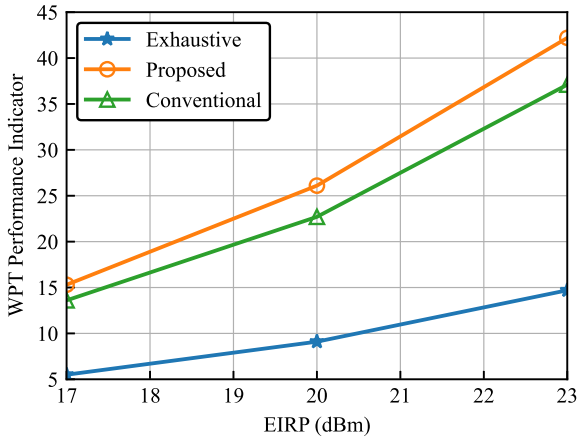

FIGURE 12. WPT performance indicator versus EIRP for Scenario 3.

during the optimal beam selection. Since the harvested energy at the WCD is directly proportional to the RSSI values, the proposed algorithm provides a trade-off between performance and complexity in practical mmWave WPT systems.

Fig. 12 shows the WPT performance indicator as a function of the EIRP at the WCS. The WPT performance indicator is defined as

$$\mathrm{WPT_{PI}} = \frac{\mathrm{RSSI}}{N_\mathrm{b}}, \tag{28}$$

where N_b denotes the number of beam allocations required for beam selection. Although the exhaustive search algorithm achieves the highest RSSI, it requires a large number of beam allocations, resulting in a lower value of the performance indicator. In contrast, the proposed algorithm achieves a higher performance indicator compared to the conventional algorithm. This observation highlights the trade-off between the performance improvement obtained by mitigating EP and the additional computational overhead.

VII. CONCLUSION

In this paper, we proposed the hierarchical beam selection algorithm for the WCS to transfer wireless power to the WCD at an arbitrary location. The proposed algorithm reduced computational complexity by hierarchically selecting the optimal beam for the WCD using L levels of beams with different beamwidths. Specifically, the verification process was proposed to mitigate EP between levels caused by incorrect optimal beam selections at each level. We implemented the proposed algorithm on the commercial mmWave RF module and validated its performance in the laboratory environment. Experimental results showed that the proposed algorithm selected the optimal beam with approximately 40 % of the computational complexity required by the exhaustive search algorithm. In addition, the verification process mitigated EP across levels compared to the conventional algorithm.

As future work, a learning-based beam selection algorithm that operates under RSSI-based feedback conditions will be investigated to further improve beam selection performance in mmWave WPT systems.

REFERENCES

[1] X. Wang, L. Kong, F. Kong, F. Qiu, M. Xia, S. Arnon, and G. Chen, "Millimeter wave communication: A comprehensive survey," *IEEE Commun. Surveys Tuts.*, vol. 20, no. 3, pp. 1616–1653, 3rd Quart., 2018.
[2] M. Wagih, A. S. Weddell, and S. Beeby, "Millimeter-wave power harvesting: A review," *IEEE Open J. Antennas Propag.*, vol. 1, pp. 560–578, 2020.
[3] Y. Motwani, K. K. Kota, and P. D. Mankar, "Sparsity-based channel estimation for RIS-aided MIMO mmWave communication systems," in *Proc. IEEE 35th Int. Symp. Pers., Indoor Mobile Radio Commun. (PIMRC)*, Valencia, Spain, Sep. 2024, pp. 1–6.
[4] H. Kong, C. Huang, J. Yu, and X. Shen, "A survey of mmWave radar-based sensing in autonomous vehicles, smart homes and industry," *IEEE Commun. Surveys Tuts.*, vol. 27, no. 1, pp. 463–508, Feb. 2025.
[5] J. Chen, Z. Ma, C. Li, M. Wang, H. Xing, W. Liang, and Y. Jiang, "Design of high-efficiency rectenna for microwave power wireless transmission systems," *ETRI J.*, vol. 46, no. 6, pp. 1103–1112, May 2024.
[6] G. N. Kamga and S. Aïssa, "Wireless power transfer in mmWave massive MIMO systems with/without rain attenuation," *IEEE Trans. Commun.*, vol. 67, no. 1, pp. 176–189, Jan. 2019.
[7] G. Kwon, H. Park, and M. Z. Win, "Joint beamforming and power splitting for wideband millimeter wave SWIPT systems," *IEEE J. Sel. Topics Signal Process.*, vol. 15, no. 5, pp. 1211–1227, Aug. 2021.
[8] M. Wang, C. Zhang, X. Chen, and S. Tang, "Performance analysis of millimeter wave wireless power transfer with imperfect beam alignment," *IEEE Trans. Veh. Technol.*, vol. 70, no. 3, pp. 2605–2618, Mar. 2021.
[9] C. Psomas and I. Krikidis, "Energy beamforming in wireless powered mmWave sensor networks," *IEEE J. Sel. Areas Commun.*, vol. 37, no. 2, pp. 424–438, Feb. 2019.
[10] J. Guo, X. Zhou, and S. Durrani, "Wireless power transfer via mmWave power beacons with directional beamforming," *IEEE Wireless Commun. Lett.*, vol. 8, no. 1, pp. 17–20, Feb. 2019.
[11] K. Tang, F. Jiao, P. Yan, Z. Wang, W. Feng, W. Che, and Q. Xue, "Energy efficiency maximization for mmWave WPCN with dynamic multi-steerable energy beamforming," *IEEE Trans. Veh. Technol.*, vol. 73, no. 12, pp. 18635–18648, Dec. 2024.
[12] S. Noh, M. D. Zoltowski, and D. J. Love, "Multi-resolution codebook and adaptive beamforming sequence design for millimeter wave beam alignment," *IEEE Trans. Wireless Commun.*, vol. 16, no. 9, pp. 5689–5701, Sep. 2017.
[13] K. Chen and C. Qi, "Beam training based on dynamic hierarchical codebook for millimeter wave massive MIMO," *IEEE Commun. Lett.*, vol. 23, no. 1, pp. 132–135, Jan. 2019.
[14] J. Yang, W. Zhu, M. Tao, and S. Sun, "Hierarchical beam alignment for millimeter-wave communication systems: A deep learning approach," *IEEE Trans. Wireless Commun.*, vol. 23, no. 4, pp. 3541–3556, Apr. 2024.

[15] C. Shao, C. Liu, L. Zhao, M. Li, X. Zhang, and M. Sun, "Deep learning-based millimeter wave beam recommendation via channel knowledge map," *IEEE Wireless Commun. Lett.*, vol. 14, no. 6, pp. 1648–1652, Jun. 2025.
[16] M. H. Hashir, Memoona, and S. W. Kim, "GPS-based beam prediction using lightweight deep learning models for mmWave networks," *IEEE Access*, vol. 13, pp. 186333–186346, Oct. 2025.
[17] M. B. Janjua, H. T. Abbas, K. A. Qaraqe, and H. Arslan, "Beam selection for ambient backscatter communication in beamspace mmWave symbiotic radio," *IEEE Wireless Commun. Lett.*, vol. 12, no. 3, pp. 560–564, Mar. 2023.
[18] A. Alkhateeb, G. Leus, and R. W. Heath, "Limited feedback hybrid precoding for multi-user millimeter wave systems," *IEEE Trans. Wireless Commun.*, vol. 14, no. 11, pp. 6481–6494, Nov. 2015.
[19] Y. Ahn, T. Kim, and C. Lee, "A beam steering based hybrid precoding for MU-MIMO mmWave systems," *IEEE Commun. Lett.*, vol. 21, no. 12, pp. 2726–2729, Dec. 2017.
[20] S. Ulukus, A. Yener, E. Erkip, O. Simeone, M. Zorzi, P. Grover, and K. Huang, "Energy harvesting wireless communications: A review of recent advances," *IEEE J. Sel. Areas Commun.*, vol. 33, no. 3, pp. 360–381, Mar. 2015.
[21] S. Boyd and L. Vandenberghe, *Convex Optimization*. Cambridge, U.K.: Cambridge Univ. Press, 2004.
[22] E. Boshkovska, D. W. K. Ng, N. Zlatanov, and R. Schober, "Practical non-linear energy harvesting model and resource allocation for SWIPT systems," *IEEE Commun. Lett.*, vol. 19, no. 12, pp. 2082–2085, Dec. 2015.
[23] *5G Antenna Module*. Accessed: Jul. 13, 2025. [Online]. Available: https://www.doosanelectronics.com/kr/product/Newbusiness_5GAntennaModule

JAE CHEOL PARK received the B.S. degree in electronics engineering and the M.S.E. degree in electronics and radio engineering from Kyung Hee University, in 2009 and 2010, respectively, and the Ph.D. degree in electrical engineering from Korea Advanced Institute of Science and Technology (KAIST), in 2024.

He is currently a Principal Researcher with the Electronics and Telecommunications Research Institute (ETRI). His research interests include the design and analysis of UAV communication systems, machine learning for wireless communication systems, and mmWave communication systems.

JUNGICK MOON received the M.S. and Ph.D. degrees in electrical engineering from the Department of Electrical Engineering, KAIST, Daejeon, South Korea, in 2000 and 2004, respectively.

Since 2004, he has been with ETRI as a Principal Researcher. His research interests include small and broadband antennas, wireless power transmission, and RF energy harvesting technologies.

JUNIL CHOI (Senior Member, IEEE) received the B.S. (Hons.) and M.S. degrees in electrical engineering from Seoul National University, in 2005 and 2007, respectively, and the Ph.D. degree in electrical and computer engineering from Purdue University, in 2015.

He is currently working as a Tenured Associate Professor with the School of Electrical Engineering, KAIST. From 2007 to 2011, he was a member of Technical Staff at the Samsung Advanced Institute of Technology (SAIT) and Samsung Electronics Company Ltd., South Korea, where he contributed to advanced codebook and feedback framework designs for the 3GPP LTE/LTE-advanced and IEEE 802.16m standards. Before joining KAIST, he was a Postdoctoral Fellow at The University of Texas at Austin, from 2015 to 2016, and an Assistant Professor at POSTECH, from 2016 to 2019. His research interests include the design and analysis of massive MIMO, mmWave communications, satellite communications, visible light communications, and communication systems using machine-learning techniques.

Dr. Choi was a co-recipient of the 2022 IEEE Vehicular Technology Society Best Vehicular Electronics Paper Award, the 2021 IEEE Vehicular Technology Society Neal Shepherd Memorial Best Propagation Award, the 2019 IEEE Communications Society Stephen O. Rice Prize, the 2015 IEEE Signal Processing Society Best Paper Award, and the 2013 Global Communications Conference (GLOBECOM) Signal Processing for Communications Symposium Best Paper Award. He was awarded the Michael and Katherine Birck Fellowship from Purdue University, in 2011, the Korean Government Scholarship Program for Study Overseas (2011–2013), the Purdue University ECE Graduate Student Association (GSA) Outstanding Graduate Student Award, in 2013, the Purdue College of Engineering Outstanding Student Research Award, in 2014, the IEEE ComSoc AP Region Outstanding Young Researcher Award, in 2017, the NSF Korea and Elsevier Young Researcher Award, in 2018, the KICS Haedong Young Researcher Award, in 2019, and the IEEE Communications Society Communication Theory Technical Committee Early Achievement Award, in 2021.